J. Fluid Mech. (2002), *vol.* 465, *pp.* 261–291.
DOI: 10.1017/S002211200200109X Printed in the United Kingdom

Granular shear flows at the elastic limit

By CHARLES S. CAMPBELL

Department of Mechanical Engineering, University of Southern California, Los Angeles, CA 90089-1453, USA

(Received 11 November 2000 and in revised form 4 January 2002)

This paper describes computer simulation studies of granular materials under dense conditions where particles are in persistent contact with their neighbours and the elasticity of the material becomes an important rheological parameter. There are two regimes at this limit, one for which the stresses scale with both elastic and inertial properties (called the elastic–inertial regime), and a non-inertial quasi-static regime in which the stresses scale purely elastically (elastic–quasi-static). In these elastic regimes, the forces are generated by internal force chains. Reducing the concentration slightly causes a transition from an elastic to a purely inertial behaviour. This transition occurs so abruptly that a 2% concentration reduction can be accompanied by nearly three orders of magnitude of stress reduction. This indicates that granular flows near this limit are prone to instabilities such as those commonly observed in shear cells. Unexpectedly, there is no path between inertial (rapid) flow and quasi-static flow by varying the shear rate at a fixed concentration; only by reducing the concentration can one cause a transition from quasi-static to inertial flow. The solid concentrations at which this transition occurs as well as the magnitude of the stresses in the elastic regimes are strong functions of the particle surface friction, because the surface friction strongly affects the strength of the force chains. A parametric analysis of the elastic regime generated flowmaps showing the various regimes that might be realized in practice. Many common materials such as sand require such large shear rates to reach the elastic–inertial regime that it is unattainable for all practical purposes; such materials will demonstrate either an elastic–quasi-static behaviour or a pure inertial behaviour depending on the concentration – with many orders of magnitude of stress change between them. Finally, the effects of nonlinear contacts are investigated and an appropriate scaling is proposed that accounts for the nonlinear behaviour in the elastic–quasi-static regime.

1. Introduction

The history of granular flow modelling begins with quasi-static flow theory (see Jackson 1983). As the name suggests these theories deal with slowly moving flows that demonstrate no velocity dependence and are usually formulated by incorporating a Coulomb failure criterion into plasticity models. Implicit in almost all of these models is that the flowing material is always at the point of incipient yield, with a ratio of maximum shear to normal stress equal to the tangent of the internal angle of friction of the material. In the last 20 years or so, there has been a great deal of development at the other end of the spectrum, in the slightly misnamed field of rapid granular flows, which would more accurately be called rapidly shearing or collisional granular flows (see the review by Campbell 1990). These theories took the point of view that in highly excited systems, the particles are reminiscent of molecules in the kinetic

theory of gases and could be analysed utilizing formalisms devised for kinetic theory. In such systems as in their molecular counterparts, transport rates are controlled by a 'granular temperature' which is a measure of the kinetic energy contained in the random motion of the individual particles. Rapid flow ideas have been shown to account for measurements of heat (Wang & Campbell 1992) mass (Savage & Dai 1993; Campbell 1997*a*) and momentum transfer (e.g. Lun *et al.* 1984; Savage & Sayed 1984; Jenkins & Richman 1985; Campbell 1989; Wang & Campbell 1992; Goldshtein & Shapiro 1995; Goldhirsch & Tan 1996). The science of rapid granular flows originated with the dense suspension experiments of Bagnold (1954), but recently Hunt *et al.* (2002) have shown that Bagnold's stress measurements are probably the results of secondary flows in his apparatus and unlikely to be related to the behaviour of dry granular materials.

However, it eventually became apparent that very few granular flows outside the laboratory were actually rapid granular flows. Strictly, rapid flows allow no enduring contacts between particles as their underlying kinetic theory framework is based on an implicit assumption of instantaneous binary collisions. (Although Hwang & Hutter 1995 have made a first-order attempt to incorporate finite collision times into rapid flow rheology.) Yet it is common experience that particles remain in contact for long periods of time even during flow. Under Earth's gravity, very large shear rates are required to maintain a rapid granular flow as the granular temperature must be large enough to generate sufficient dispersive pressure to support the weight of the material. In the shear cell studies that lead to Wang & Campbell (1992), it was difficult to maintain rapid flows below $70\,\mathrm{s}^{-1}$ of shear rate – an indication of the large shear rates required.

The current study was engendered by three previous studies that the author participated in. The first of these concerned the phase change between fluid-like and solid-like behaviour of granular materials (Zhang & Campbell 1992; Campbell & Zhang 1992; Campbell 1993), which indicated that this transition could not be described in terms of rapid granular flow ideas (as first proposed by Jenkins & Askari 1991), but instead demonstrated a quasi-static yield behaviour. However, later studies on hoppers (Potapov & Campbell 1996), which are clearly not rapid granular flows, indicated that the generally accepted assumption of quasi-static yield occurring at the internal angle of friction of the material could not explain the stress state within the hopper. In particular, standard quasi-static flow analyses assume that the ratio of maximum shear to normal stress should equal the internal angle of friction, which is treated as a material property. However the Potapov & Campbell (1996) results showed that this ratio was far from constant and reached its maximum value in the hopper throat. Finally, large-scale computer simulations of landslides, performed by Campbell, Cleary & Hopkins (1995), indicated that the ratio of shear to normal stress on the base of the slide increased with the shear rate (i.e. the velocity gradient at the slide's base) even though both rapid flow and quasi-static flow theories suggest that this ratio should be independent of shear rate. This was an indication that the landslides were occurring in a new regime that is neither rapid nor quasi-static. Furthermore, these observations were consistent with the hopper simulation mentioned above, as the largest stress ratios were found in the hopper throat where the shear rates are the largest (as the velocities are highest and the channel is the most narrow). In the phase-change simulations, the stress ratio could also be interpreted as increasing with the shear rate. However, it was difficult to obtain rheological information from these studies as neither the density or the shear rate could be sufficiently controlled.

This led to the current investigations which were originally designed to quantita-

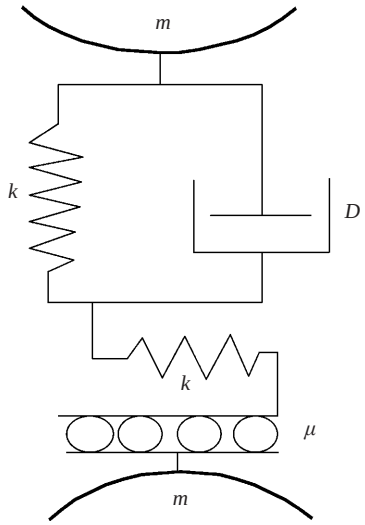

FIGURE 1. A schematic of the particle contact model.

tively determine the effect of shear rate on the stresses in dense granular flow and, in particular, on the shear-to-normal stress ratio at controlled shear rates and concentrations. The original goal was to look for flow regimes where the shear-to-normal stress ratio varied with shear rate as observed in the three studies mentioned above. Such a regime was found but, as shall be seen, cannot explain all of those observations.

This work was performed using a soft-particle computer simulation that is described in the next section. Section 3 introduces the elastic–inertial and elastic–quasi-static flow regimes which are central to this paper, along with the dimensionless parameters that govern elastic granular flows. A broader view is presented in § 4 allowing observations of the transitions from inertial to elastic behaviour. This is followed by a discussion in § 5 that attempts to explain where the various flow regimes are likely to be found in practice by analysing the appropriate elastic parameter. Finally, § 6 presents a scaling that accounts for the effects of nonlinear stiffness in the elastic–quasi-static regime.

Preliminary reports of this work can be found in Campbell (2001*a*, *b*).

2. Computer simulation

These studies were performed using soft-particle computer simulations (see the reviews of computer simulation techniques by Campbell 1986, 1997*b*, and Herrmann & Luding 1998). The soft-particle technique generally models the interaction between particles as a spring (which may be linear or nonlinear) in the direction along the particle centres that acts as long as the particles remain in contact. Some mechanism is also added in parallel to the spring to dissipate the collisional energy and here, as in the original work of Cundall & Stack (1979), this is accomplished by putting a viscous dashpot in parallel with the spring. The contact model is schematically illustrated in figure 1. The spring has an associated stiffness k, which will be varied throughout this work. The stiffness k may be linear or nonlinear, but linear springs are used throughout this work except in § 6. Each time k changes, the dashpot coefficient D is simultaneously varied to keep a constant binary coefficient of restitution ε (the ratio of recoil to impact velocity for a binary collision in the centre-of-mass frame). For a

linear spring, the coefficient of restitution is given by

$$\varepsilon = \exp\left[-\frac{\pi D}{\sqrt{2mk - D^2}}\right], \tag{2.1}$$

where m is the particle mass. Note that even though few flows presented in this paper are collisional, the coefficient of restitution is still a convenient dimensionless representation of the particle inelasticity with an easily understood physical meaning and, as will be seen, appropriately scales the dashpot coefficient D. In the direction tangential to the contact point the particles are connected to a frictional slider with an associated friction coefficient μ, connected in series with another spring also with stiffness k. (Thus as the particle surfaces move relative to one another in the direction tangential to the contact point, the tangential spring will load until the tangential force reaches the friction coefficient times the normal force, at which point the surfaces slip relative to one another against a force equal to μ times the normal force.)

The simulation consists of simultaneously integrating all of the equations of motion for all the particles in the system with forces derived from the contact model shown in figure 1. A standard second-order time-stepping scheme is used for the integration with a time step of $\mathrm{d}t = 0.02\pi/\sqrt{2k/m - D^2/m^2}$ which corresponds to one fiftieth of a binary collision time.

One thousand spheres of diameter d were used in all these simulations, with the exception of a few simulations performed to test the sensitivity of the results to the size of the simulation. The particles are confined in a cubical control volume with dimensions roughly $10 \times 10 \times 10$ mean particle spacings at whatever particle concentration is required. The volume is kept fixed throughout the simulation. In the following, x is used to represent the direction of the mean motion, y is the direction of the velocity gradient (so the shear rate $\gamma = \mathrm{d}u_x/\mathrm{d}y$, where u_x is the mean velocity in the x-direction), and z represents the coordinate out of the shear plane. The control volume was bounded in all directions by periodic boundaries. For a classic periodic boundary, when a particle passes through one boundary it re-enters from the opposite side with exactly the same position and velocity with which it left; this simulates a situation where the control volume and every particle within it are periodically repeated infinitely many times in all directions, so that, for example, as a particle passes out through the downstream boundary, it passes into the downstream periodic image and is replaced by a particle entering from the upstream periodic image. However, to obtain rheological information, it is convenient to induce a uniform shear within the control volume so as to help isolate the effect of shear rate. To do this, the periodic images above and below the control volume in the y-direction are set in motion with fixed velocity in the manner originally used by Lees & Edwards (1972). It was found that uniform shearing could be achieved in these systems up to a solids concentration of $\nu = 0.62$, where ν is the solid volume fraction. Beyond that concentration, the shearing generally took on a shear-band type of deformation with only a small part of the material undergoing shear.

For the initial state of the system, the particles are positioned randomly within the cell and the shear flow is allowed to distribute them as it will, so that the particle configuration is eventually determined by the concentration and necessity of conforming to a shear flow. This is difficult to arrange at large solids concentrations when particles are in contact. To achieve this, the particles were inserted at random positions (chosen by a random number generator) but at one-half their desired radius (i.e. at an initially small concentration). Then the shear flow was set in motion and during the early stages of the simulation, the particles were grown to their final

diameters. Note that this technique is essentially the same as starting the particles in a control volume with each linear dimension doubled and then shrinking the control volume.

Several other techniques were examined for generating the initial state of the system using full sized particles arranged in regular configurations including face-centred cubic, triangular prismatic (with generators in the direction of flow) and rhombohedral packings. The first two have symmetry planes oriented in such a way as to allow easy shearing. Such systems could run for long periods of time generating very little stress. However, the regular packing was always observed to break down accompanied by a dramatic increase in the stresses; this was probably a result of the strong frictional interaction in these dense system. After the breakdown, the generated stresses were for all intents and purposes identical to those generated by the randomly distributed growing particle scheme described above. For the rhombohedral packing, which has no planes of symmetry in the direction of the shear motion, the stresses generated were also identical to those generated by randomly distributed growing particles. Finally, it should be noted that the geometry of the periodic cell may preclude the system from assuming a regular packing. For example, face-centred cubic or triangular prismatic packings will not evenly fill cubic cells. Consequently, a few simulations were performed with initial particle configurations generated by the random-growing technique, but in cells whose geometry conformed to face-centred cubic or triangular prismatic packings, in order to see if the system would naturally fall into the regular packing. This was never observed. Thus, it appears that the initial arrangement of the particles has no effect on the stresses which are ultimately generated by the system.

The spring/dashpot contact model shown in figure 1 is carefully chosen for these studies as they are designed to examine cases where the bulk granular material is responding elastically to the applied forces. In such a system, the Young's modulus of a bulk material consisting of many such particles is proportional to the stiffness k (for systems of particles, the relationship was derived by Bathurst & Rothenburg 1988, but has its roots in the lattice models of Cauchy 1828). The stiffness k between real solid particles is strongly dependent on the geometry of, and pressure on, the contact and is thus not solely determined by the elastic moduli of the solid material that makes up the particles. As a result k, and not the elastic properties of the constituent solid, is the important parameter in determining the elastic behaviour of the bulk material. The spring/dashpot model has the advantage over more complicated models such as the two-spring model of Walton & Braun (1986) that it has only a single spring constant which may then be used as a characteristic scale of the problem. For the same reason, only monodispersed spheres are studied as that allows the particle diameter d to be used as a well-defined intrinsic length scale.

For these studies, the same stiffness k is used in both the normal and tangential directions. Largely this was done so that there would be only a single stiffness which could then be used as a scaling parameter. However, this choice may be critical to this study because of the elastic nature of the generated stresses. As Bathurst & Rothenburg (1988) show that the ratio of the tangential to the normal stiffness, k_T/k, determines the Poisson's ratio of the bulk granular solid, tests were performed to assess the affect of changing this ratio. The results showed that it has a very weak effect on the magnitude of the stresses, similar to that by varying the surface friction coefficient μ (although much weaker), and only makes a significant difference when it has small values (less than 0.3). This should not be surprising as the tangential spring is connected in series with the frictional slider so one would expect some similarity in

their effects; in particular, setting the tangential stiffness to zero would be equivalent to setting $\mu = 0$. However, one might expect from the Bathurst & Rothenburg results that changing k_T/k would affect the ratio of shear to normal stress τ_{xy}/τ_{yy} in much the same manner as changing the Poisson's ratio would alter the ratio of stresses in an elastic solid. But no such variation was observed. In fact, τ_{xy}/τ_{yy} seemed independent of k_T/k even though the magnitudes of τ_{xy} and τ_{yy} were not. Thus, for the problems studied here, the tangential stiffness is not a significant parameter and no significant physics are lost by assuming it equal to the normal stiffness.

One advantage of a linear contact (k = const.) in the contact model shown in figure 1 is that any binary collision between particles will have a fixed contact time:

$$T_{bc} = \frac{\pi}{\sqrt{2k/m - D^2/m^2}}. \tag{2.2}$$

As in Campbell (1993) and Potapov & Campbell (1996) the value of the average actual contact time relative to T_{bc} may be used as an indicator of whether the material is behaving in a collisional (rapid flow) manner. In an ideal collisional system, the contact time must equal the binary collision time. Longer contact times are only possible if more than two particles interact simultaneously. One can imagine a scenario in which two particles come into contact, but before they come apart, a third particle collides and pushes them back together, extending the collision time. During that exchange, momentum is transmitted elastically through the particle contacts at a rate determined by the contact stiffnesses. Note that this violates the assumptions of rapid flow theory which assumes that the transport rates are governed solely by the granular temperature as in a gas, and not at rates governed by the particle elasticity as in an elastic solid.

These simulations are best thought of as computational experiments. Once the particles are placed in the control volume and the boundaries set in motion, the simulation proceeds as it will. Once statistically stationary conditions are reached, the properties of the simulation are sampled and averaged over time for whatever information is desired, in this case the stress state. The averaging time is taken to be long enough so that the sampled stresses are no longer significantly changing with time. Typical averaging times were $\gamma t = 300$, but some went as high as $\gamma t = 10\,000$, or particularly for the smallest shear rates, as low as $\gamma t = 50$.

There are two mechanisms by which the stresses are generated and the techniques for finding them are by now fairly standard. The 'contact stresses' reflect the force transmitted across interparticle contacts and can be found by taking the average $\langle \boldsymbol{F}\boldsymbol{l} \rangle$, where $\boldsymbol{F}$ is the vector force between the particles (which includes both compression and frictional forces), $\boldsymbol{l}$ is the vector connecting the particle centres and $\langle\ \rangle$ represents a time average over all the particle contacts in the control volume. The 'streaming stresses' reflect the momentum carried by the unsteady motions of particles as they move through the system. In form, they appear as Reynolds stresses, $\rho v \langle \boldsymbol{u}'\boldsymbol{u}' \rangle$, where ρ is the solid particle density, v is the solid concentration (so ρv is the bulk density) and $\boldsymbol{u}'$ is the fluctuating particle velocity (determined as the r.m.s. value of the difference between the instantaneous particle velocity and the velocity of the imposed shear flow). The streaming stresses are small at the high concentrations studied here, but are still sampled and included in the results.

The effect of control volume size was tested by examining cubical control volumes ranging in size from $5 \times 5 \times 5$ mean particle spacings up to $20 \times 20 \times 20$, and non-cubical volumes with the largest such simulation having $7 \times 100 \times 7$ mean particle spacings with the largest dimension in the direction of the velocity gradient. (Note

the numbers are listed as the number of particles in the x-, y- and z-directions respectively where the velocity gradient points in the y-direction.) All of these early test simulations were performed at a solid concentration of $\nu = 0.6$, and a friction coefficient, $\mu = 0.5$. No effect was found on the final stress results as long as the dimensions were at least $7 \times 7 \times 7$; the $10 \times 10 \times 10$ size, used for all these data, was chosen to be somewhat larger than that minimum value. (Further size tests were performed to look for possible size effects on the points of transition in the flow behaviour. These will be discussed later in the paper, although again no size effects were found.)

The volume remains constant throughout all of these flows so that the solid fraction remains a fixed, non-fluctuating constant. It should be noted that the stresses arise from the necessity to shear the material at a fixed solid concentration. Simulations which are started with no shearing motion generate no stresses as the solid fraction is below a random close pack and the growing particles naturally assume configurations where they are not in contact with their neighbours. This is probably because the growth of the particles will gently push the neighbouring particles away, leaving a configuration where no particles are in contact.

3. Preliminary observations of elastically dominated granular flows

The hopper, landslide and phase-change simulations referred to above all indicate that the apparent friction coefficient, τ_{xy}/τ_{yy}, changes with the shear rate γ. At the outset, this presents a dimensional problem as γ has units of $(\text{time})^{-1}$, while the stress ratio τ_{xy}/τ_{yy} is dimensionless and can thus only be a function of dimensionless parameters. Note that the inverse shear rate represents the only time scale in rapid granular flow theory, while no time scale appears in quasi-static theories. Thus some other parameter must be introduced into the analysis which contains units of time by which the shear rate can be scaled. The only possible candidates come from the particle contact model. As the particle surface friction and the coefficient of restitution are dimensionless, the most likely remaining possibility is the contact stiffness, k. A stiffness scaled with the shear rate has the form

$$\frac{k}{\rho d^3 \gamma^2}. \tag{3.1}$$

Note that this is similar to the parameter B, studied by Babic, Shen & Shen (1990).

A time scale also exists from the viscous damping in the contact model. Choosing k to supply the time scale implicitly assumes that the effect of the viscous damping is completely accounted for by the coefficient of restitution, ε as given in (2.1). This assumption can be tested by working with different diameters, shear rates and stiffnesses that yield the same $k/(\rho d^3 \gamma^2)$ but, as can be seen from (2.1), require different D to maintain the same ε. This was done throughout this work and when properly scaled (in the manner discussed below), the resultant stresses and stress ratios overlapped nearly exactly which indicates that no other parameter makes a significant contribution.

Figure 2 shows a plot of the shear to normal stress ratio τ_{xy}/τ_{yy} as a function of $k/(\rho d^3 \gamma^2)$ at a constant solid concentration, $\nu = 0.6$, particle surface friction coefficient $\mu = 0.5$, and for three different coefficients of restitution, $\varepsilon = 0.1$, 0.7 and 1.0. The concentration $\nu = 0.6$ is used for these preliminary studies as all of the cases discussed above, phase-change, hoppers and landslides operate near the shearable limit (about $\nu = 0.63$). From the form of $k/(\rho d^3 \gamma^2)$ it can be seen that increasing the stiffness k

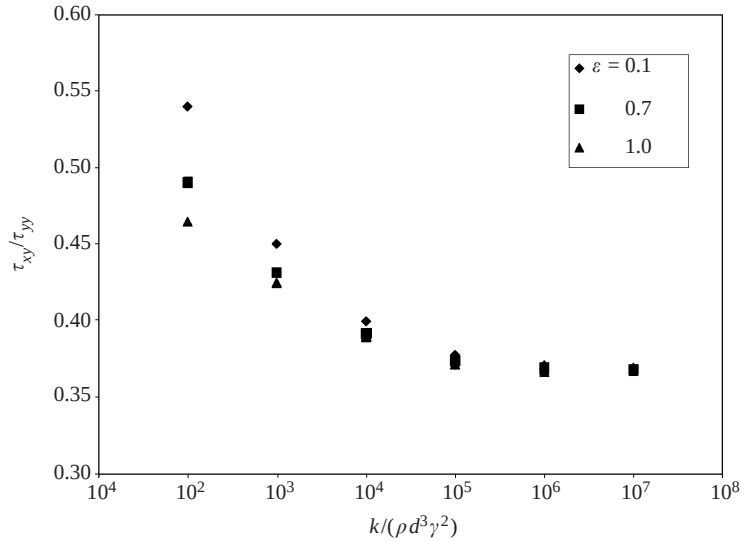

FIGURE 2. The ratio of shear to normal stress, τ_{xy}/τ_{yy}, as a function of the parameter, $k/(\rho d^3\gamma^2)$. All of these data were taken from 1000-particle computer simulations at a constant solid concentration, $\nu = 0.6$ and particle surface friction, $\mu = 0.5$ for three different values of the coefficient of restitution, ε. Note that τ_{xy}/τ_{yy} decreases with $k/(\rho d^3\gamma^2)$ (i.e. increasing k, decreasing γ) eventually approaching a constant value indicative of quasi-static behaviour.

moves one from left to right on the figure, while increasing the shear rate γ moves one from right to left. One can see that for the lower values of $k/(\rho d^3\gamma^2)$, the values of the stress ratio τ_{xy}/τ_{yy} drop with increasing $k/(\rho d^3\gamma^2)$ (i.e. with increasing k or with decreasing, γ). For large values of $k/(\rho d^3\gamma^2)$ (i.e. large k, small γ) the stress ratio becomes constant which is indicative of the quasi-static behaviour; quasi-static flow should be expected as this limit corresponds to zero shear rate. Note that the coefficient of restitution ε is only important at small $k/(\rho d^3\gamma^2)$, which might be expected as this corresponds to conditions of large shear rates with correspondingly large impact velocities, which will generate large dashpot forces from the contact model shown in figure 1.

Thought of as a dimensionless shear rate, the effect of $k/(\rho d^3\gamma^2)$ on τ_{xy}/τ_{yy} fits the basic understanding of quasi-static (small γ) and inertial (large γ) behaviour. But if thought of as a dimensionless contact stiffness, k, the behaviour somewhat contradicts that picture. Large k implies a shorter binary contact time and approaches the instantaneous contact time assumption implicit in rapid-flow theories; yet increasing k (leading to large $k/(\rho d^3\gamma^2)$) corresponds to more quasi-static behaviour. This apparent contradiction will be resolved in the next section, which will show that the collisional and quasi-static limits are separated, not by shear rate, but by concentration. There it will be shown that at the larger ν, increasing $k/(\rho d^3\gamma^2)$ approaches the quasi-static limit (as shown in figure 2), but at only slightly smaller ν, the flow approaches collisional behaviour at large $k/(\rho d^3\gamma^2)$. Thus both interpretations of $k/(\rho d^3\gamma^2)$ are correct, but under different circumstances.

Figure 2 (and for that matter, figures 3–5) also demonstrates that the scaling of the problem is dependent on the dashpot coefficient, D, only through the coefficient of restitution ε. Except for the two extreme values of $k/(\rho d^3\gamma^2)$, two and in some cases three stiffnesses, varying over 2–3 orders of magnitude, and three particle diameters, varying over a factor of 4, were used for each combination of $k/(\rho d^3\gamma^2)$ and ε in

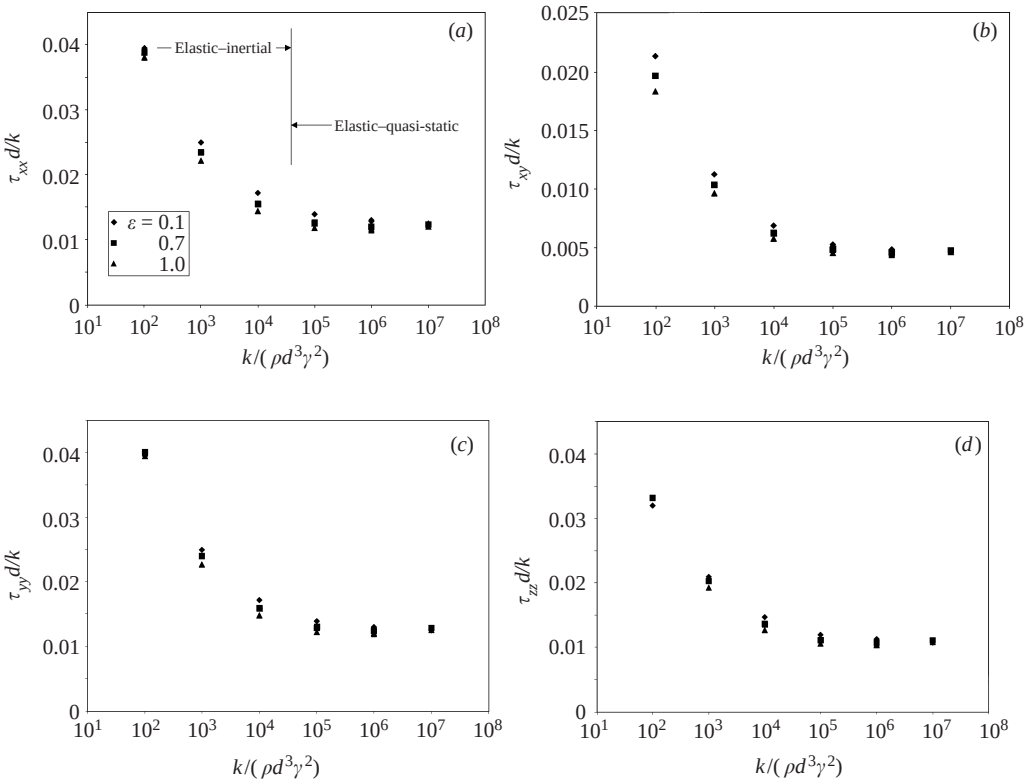

FIGURE 3. The individual components of the stress tensor scaled by the particle stiffness, $\tau_{ij}d/k$, for the data plotted in figure 2 ($\nu = 0.6$, $\mu = 0.5$). (*a*) τ_{xx}, (*b*) τ_{xy}, (*c*) τ_{yy}, (*d*) τ_{zz}. Note that the data scale with the stiffness indicating that the stresses are generated by the elasticity of the material. Panel (*a*) schematically illustrates the division of the regimes into elastic–inertial and elastic–quasi-static.

this figure. Except for some slight elongation of the square-shaped points, which is the only apparent manifestation of the corresponding data scatter, the points overlap almost exactly. This demonstrates the robustness of the dimensional scaling of the problem. Notice that from equation (2.1), if ε is to be held constant then D must be changed every time that k changes. Yet there is no resultant scatter in the results, indicating that all the dimensional effects of changing D are accounted for by the coefficient of restitution ε.

Figure 3 shows the individual stresses scaled by the stiffness, $\tau_{ij}d/k$. Again, these data were generated for two (and in some cases, three) different values of the stiffness k, and three particle diameters d, although this is not apparent in the figure as the values overlay one another almost exactly. Notice that both quantities decrease with $k/(\rho d^3\gamma^2)$, becoming constant at large $k/(\rho d^3\gamma^2)$, just as for the stress ratio, τ_{xy}/τ_{yy}. Note also that all the stress components vary with the coefficient of restitution ε in a manner qualitatively similar to the stress ratio shown in figure 2 although the shear stress τ_{xy} is more strongly dependent on ε than any of the normal stresses.

As the stresses scale with the particle stiffness k, the rheology is dominated by the particle elasticity. Furthermore, as illustrated in figure 3(*a*), the flows can be further subdivided into an 'elastic–inertial' regime in which the stresses scale elastically but also increase with shear rate. This corresponds to the region $k/(\rho d^3\gamma^2) < 10^5$. For $k/(\rho d^3\gamma^2) > 10^5$ the stresses again scale elastically but are strain-rate independent

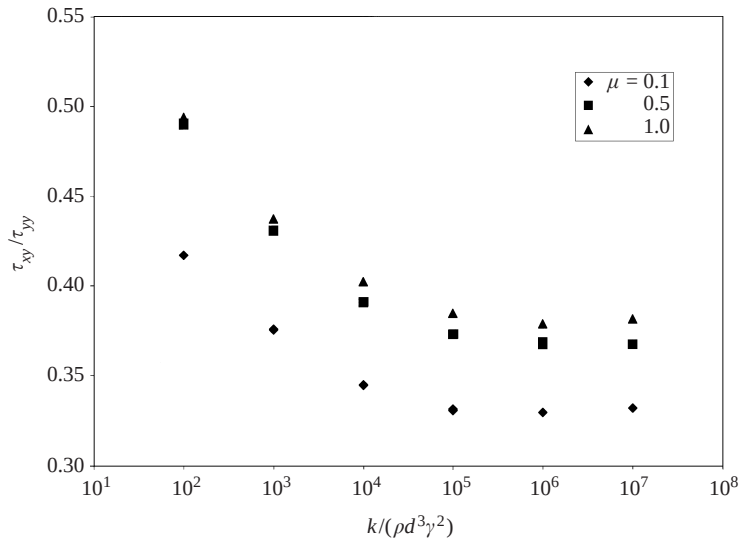

FIGURE 4. The effect of particle surface friction on the stress ratio τ_{xy}/τ_{yy}, from 1000-sphere simulations at a concentration $\nu = 0.6$.

forming an 'elastic–quasi-static' regime. It is worth noting that the stresses in the elastic–inertial regime increase linearly proportional to the shear rate (i.e. proportional to $(k/(\rho d^3\gamma^2))^{-1/2}$). As they do not increase proportional to the square of the shear rate they cannot be thought of as the sum of a quasi-static stress and a Bagnold-like inertial stress. In particular, increasing the shear rate (decreasing $k/(\rho d^3\gamma^2)$) does not cause a transition from a quasi-static behaviour to a Bagnold-like behaviour. This is counter to the general assumption that quasi-static behaviour is to be expected at small shear rates and a Bagnold-like behaviour is to be found at large shear rates. While a flow regime transition is observed by changing the shear rate, the transition is between quasi-static behaviour and a third flow regime, the elastic–inertial.

The effect of the particle surface friction μ is shown in figures 4 and 5. For a rapid granular flow, the surface friction largely affects only the energy dissipation (at least far from solid boundaries), so that for a given shear rate and concentration, the larger the surface friction, the larger the energy dissipation and, consequently, the smaller the granular temperature and all of its associated transport rates. But overall this effect is weak. It is not surprising that a much stronger effect might be felt at large concentrations where one can expect enduring contacts, and thus a greater sensitivity to the details of the contact model. Along those lines, figure 4 shows a relatively strong effect of the surface friction on the stress ratio τ_{xy}/τ_{yy}. As might be expected expected, τ_{xy}/τ_{yy} increases with μ. But notice that while there is a significant change in τ_{xy}/τ_{yy} on increasing μ from 0.1 to 0.5, there is a relatively minor change going from $\mu = 0.5$ to 1.0. (Note: curve fitting shows that all the lines will collapse together by plotting $(\tau_{xy}/\tau_{yy})^{-0.085}$ as a function of $k/(\rho d^3\gamma^2)$.)

Much more interesting is the effect on the normal stress $\tau_{yy}d/k$ plotted in figure 5. In particular, in the quasi-static limit (large $k/(\rho d^3\gamma^2)$) the low friction case $\mu = 0.1$, shows almost no generated normal stress (in fact, the $\mu = 0.1$ stresses at $k/(\rho d^3\gamma^2) = 10^7$ are about 350 times smaller than those for $\mu = 0.5$ or 1.0). This indicates the ultimate source of the stresses in this elastic limit are the 'force chains' that form within a dense granular material (see for example Cundall & Strack 1979; Drescher & De Josselin

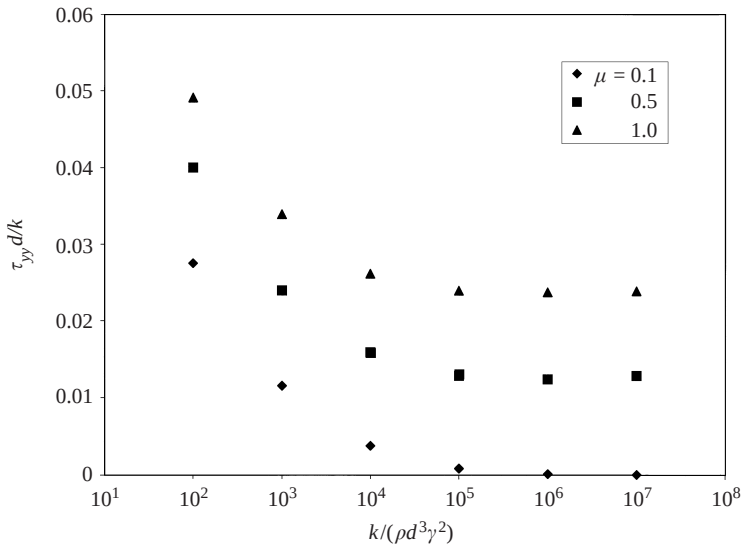

FIGURE 5. The effect of particle surface friction on the scaled normal stress $\tau_{yy}d/k$ for the data presented in figure 4. Surprisingly, there is a very strong effect of μ on the normal stress. In fact the normal stress for $\mu = 0.1$ almost disappears in the quasi-static limit (large $k/(\rho d^3\gamma^2)$). This indicates that the stress is supported by elastic particle networks whose strength depends on their structural integrity which is strongly affected by μ.

de Jong 1972; Mueth, Jaeger & Nagel 1998). These are networks of particles with heavily loaded contacts that transmit force elastically through the system. Their elastic nature is evident as force chains are experimentally detected using photoelastic techniques. In a shearing system, the shear motion will force chains to form, rotate and compress, a process that eventually causes the chains to break and collapse. After collapse, the potential energy of the contacts is converted to the kinetic energy of the particles which is quickly dissipated by the contact inelasticity and friction. (This process has been visualized in a two-dimensional photoelastic system by Howell, Behringer & Veje 1999*a*, *b*. It is nearly identical to Bonnecaze & Brady's 1992 model of electrorheological fluids except that there the particle interaction is a conservative electrical force, while here it is a conservative elastic force.) The concentration $\nu = 0.6$ used for all of these examples is smaller than the concentration of a random close pack of uniformly sized spherical particles; as a result, there are possible configurations for which the particles are not in intimate contact and thus may not be able to generate a normal stress unless something (in this case the shear flow) forces them together. The ultimate strength of the chains, i.e. the maximum load they can support before breaking, is strongly affected by the interparticle friction. For the small-friction $\mu = 0.1$ cases shown in figure 5, these chains are weak and can only support very weak forces before the structure fails. Specifically, at large values of $k/(\rho d^3\gamma^2)$, only weak force chains form and little normal force can be supported before they break.

The effect shown here cannot be simply related to the friction coefficient, μ. Unlike the τ_{xy}/τ_{yy} plot shown in figure 4, it is not possible to collapse these curves together by plotting the data in the form $(\tau_{yy}d/k)f(\mu)$ as a function of $k/(\rho d^3\gamma^2)$; this can be easily seen as at $k/(\rho d^3\gamma^2) = 10^7$ the stresses for $\mu = 0.1$ are about 350 times smaller than those for $\mu = 1.0$, whereas they are only about 1.8 times smaller at $k/(\rho d^3\gamma^2) = 100$.

The effect of the friction coefficient can be observed directly by examining the time

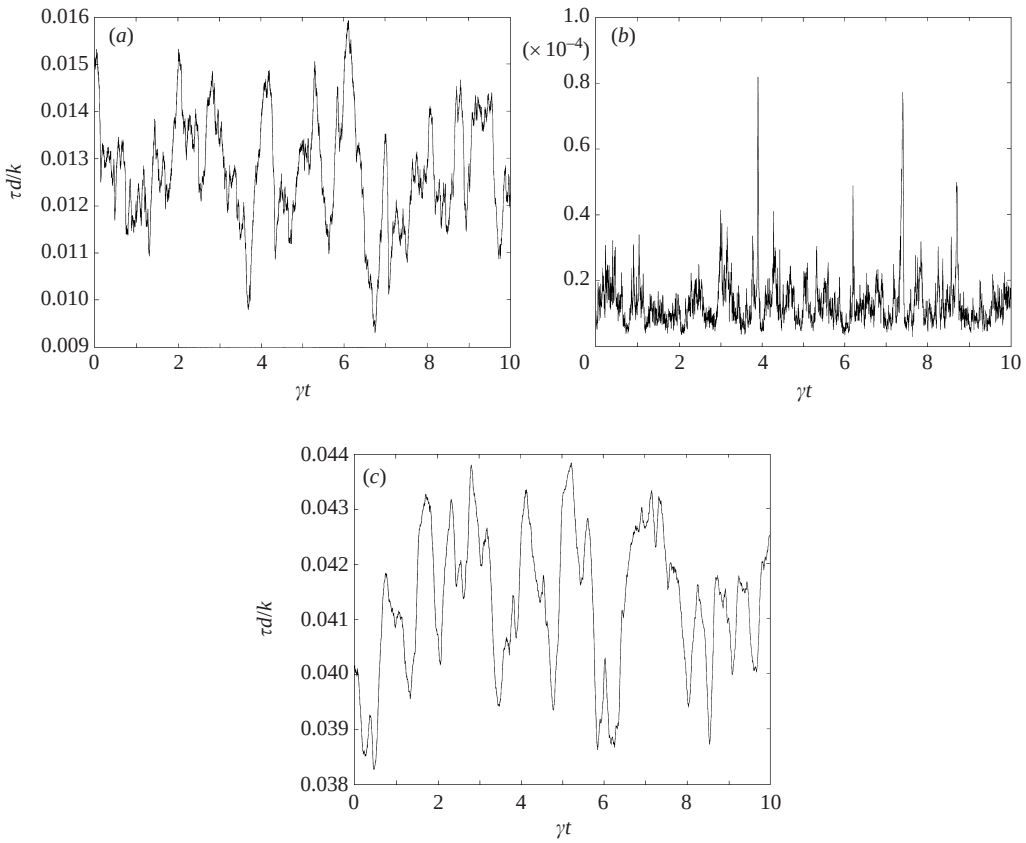

FIGURE 6. Time traces of the scaled contact normal stress, $\tau_{cyy}d/k$, plotted as functions of dimensionless time γt at $\nu = 0.6$. (*a*) $\mu = 0.5, k/(\rho d^3\gamma^2) = 10^7$, (*b*) $\mu = 0.1$, $k/(\rho d^3\gamma^2) = 10^7$, (*c*) $\mu = 0.5$, $k/(\rho d^3\gamma^2) = 100$. Cases (*a*) and (*b*) lie far out in what should be the elastic–quasi-static regime while (*c*) lies in the elastic–inertial regime. Note that the scale of (*b*) is magnified 160 times over that of (*a*) and that the largest value in (*c*) is nearly 3 times that in (*a*).

traces of the contact normal stress $\tau_{cyy}d/k$ (these are only the stresses generated by interparticle contacts) corresponding to $k/(\rho d^3\gamma^2) = 10^7$, that are shown in figure 6(*a*) and 6(*b*). Figure 6(*a*) shows the case for $\mu = 0.5$ while figure 6(*b*) shows the corresponding case for $\mu = 0.1$; note that the vertical scale on figure 6(*a*) is 160 times larger than that for figure 6(*b*). Both show a fluctuating spiked behaviour that results from the formation and breakage of the internal force chains or at least of multiparticle structures that may be precursors to force chains. Such temporally fluctuating forces have also been observed experimentally by Miller, O'Hern & Behringer (1996), and Howell, Behringer & Veje (1999*b*). Fluctuations that are qualitatively similar to figure 6(*b*) have been observed in rapid flow, e.g. Glasser & Goldhirsch (2001).

For the $\mu = 0.1$ plot shown in figure 6(*b*), the peaks are not only orders of magnitude weaker, they also persist for a much shorter time. The difference will be explained in the next section, which will show that the $\mu = 0.1$ flows are behaving inertially while the $\mu = 0.5$ flows are behaving elastically. However, because the peaks in figure 6(*b*) are much wider than the binary collision time (on this scale $\gamma T_{bc} = 0.0005$ and is essentially invisible in figures 6*a* and 6*b*) it is clear they are generated from multiparticle interactions that can only be viewed as an attempt of

the material to form force chains. The shearing of the material results in compression of the chains and the generation of the resultant stresses. Thus for $\mu = 0.5$, the force chains are stronger and persist for longer periods of time before breaking. The longer life of the force chains allows the shear to compress them to a greater extent, resulting in the larger stresses. In this way, long structural life and large stresses go hand in hand.

Figure 6(*c*), again shows $\nu = 0.6$, $\mu = 0.5$ data, but this time from the elastic–inertial regime at $k/(\rho d^3\gamma^2) = 100$. Notice that despite the slightly larger stresses (which simply reflects the difference in the mean stresses shown in figure 3*c*) the plot is very similar to figure 6(*a*). But because of the larger shear rate used in this simulation (about 100 times larger than those in figures 6*a* and 6*b*), the actual time period shown is 100 times shorter. But note that when scaled in this way, the duration of the peaks is about the same in figures 6(*a*) and 6(*c*). This indicates that, despite the different flow regime, the stresses in both cases are generated by the formation, rotation and destruction of force chains. Note that γt represents the strain so these figures indicate, as might be expected, that this process depends on the strain and not on the strain rate.

This provides the key to understanding elastic–quasi-static and elastic–inertial behaviour. Increasing the strain rate causes the force chains to form faster and more frequently (at a rate proportional to the strain rate), but persist for shorter times (a time inversely proportional to the strain rate as will be shown in figure 9 below) so that the time-averaged stress remains strain rate independent. The magnitude of the generated forces is proportional to the degree to which the chains are compressed by having to conform to a shear motion under the constraint of constant solid concentration. The interparticle forces are generated by geometric constraints and are therefore shear-rate independent. The elastic–inertial behaviour can be understood as the rising importance of additional inertial forces in the same context. Inertia can be imagined to contribute to the magnitude of the interparticle forces in the following way. As the chain forms, it will gather fast- and slow-moving particles together and by decelerating or accelerating the particles as required, force them to conform to the motion of the chain. The magnitude of this extra momentum and thus the additional interparticle force generated would be proportional to the shear rate γ. Now imagine the process of formation, growth and destruction of a chain via a shear motion. If e is the shear strain of the chain (i.e. e is the time integral of γ since the time the chain was formed) then the force, F, can be expected to vary as $F = ae + b\gamma$ where a and b are functions of the material properties and concentration. Averaging over the life of the chain yields $\langle F\rangle = a\langle e\rangle + b\gamma$. As before, the chain formation rate is proportional to γ, but the chain duration is proportional to $1/\gamma$. The stress τ is proportional to $\langle F\rangle$ and will have the form $\tau = A + B\gamma$. Thus one can anticipate quasi-static behaviour until $B\gamma$ becomes significant, and a linear increase with shear rate thereafter – exactly as observed in figures 2–5. Note that this also explains the weak effect of the coefficient of restitution seen for small values of $k/(\rho d^3\gamma^2)$ in figures 2 and 3; only at large γ are the impact velocities large enough so that the viscous damping significantly affects the applied forces.

Note that the scaled duration of the peaks in figure 6(*c*) appear to be slightly longer than those in figure 6(*a*). This will be partially explained in § 5. There it will shown that for the conditions in figure 6(*c*), the time it takes a chain to destruct, proportional to the rate at which particles elastically repel each other (which is related to the binary collision time), is becoming a significant fraction of the life of the chain. As that process depends on the elastic properties and not on the shear rate (which

governs all the other processes in the life of a force chain) the chain duration when scaled by the shear rate will be slightly longer for higher shear rates (i.e. at the smaller $k/(\rho d^3\gamma^2)$). (Note, due to the increased shear rate used to derive this plot, $\gamma T_{bc} = 0.16$ on this scale and is more noticeable than in figures 6(a) and 6(b).)

The forces in figures 6(a) and 6(c) are quite large – especially if one recognizes that $\tau d/k$ can be thought of as a dimensionless contact displacement. This can be easily seen by remembering that figure 6 shows only contact forces and that the force on a contact will appear as a stress acting over an area of the order of the projected area of a particle. Then $\tau d^2 \sim k\delta$ where δ is a characteristic contact displacement. Rearranging gives $\delta/d \sim \tau d/k$. Thus the largest peaks in figures 6(a) and 6(c) correspond to displacements of the order of 1.6% and 4.4% of a particle diameter, indicating the great strength of the force chains. Note that because the stiffness has been scaled out of the problem, this is not a result of using soft particles, but comes from the geometric restrictions of a constant-volume shear flow. (Note also that only very small volume changes would be required to relax these forces.) These forces are large enough to shatter brittle particles and, indeed, handling induced particle attrition is a constant industrial problem resulting in large monetary losses.

4. The transition between pure inertial and elastic flow

At this point, a picture begins to emerge that suggests a dimensional analysis of the form

$$\tau = f(\nu, k, \gamma, d, \rho, \mu, \varepsilon), \tag{4.1}$$

which has two equivalent non-dimensional scalings for the stress. The first would be to use a purely inertial scaling:

$$\frac{\tau}{\rho d^2\gamma^2} = f\left(\frac{k}{\rho d^3\gamma^2}, \nu, \mu, \varepsilon\right). \tag{4.2}$$

The second would be to scale the stresses with the interparticle stiffness as was done in the last section:

$$\frac{\tau d}{k} = f\left(\frac{k}{\rho d^3\gamma^2}, \nu, \mu, \varepsilon\right). \tag{4.3}$$

Note that these two scalings are simply related as $\tau/(\rho d^2\gamma^2) = (k/(\rho d^3\gamma^2))(\tau d/k)$.

Now there are two implicit limits with these scalings. The first is the pure inertial flow limit where the rheology becomes independent of the stiffness k. Such a region can be anticipated in the limit of collisional behaviour, where it is possible to compute the result of a collision purely from momentum considerations without any consideration of the stiffness or any other details of the collision. However, inertial behaviour may extend beyond the pure collisional limit and thus this scaling by itself does not imply that the flow is a rapid flow. In the inertial limit, the stiffness k and thus $k/(\rho d^3\gamma^2)$ must disappear as parameters, leaving

$$\frac{\tau}{\rho d^2\gamma^2} = f(\nu, \mu, \varepsilon). \tag{4.4}$$

The second is the elastic–quasi-static limit where the rheology becomes independent of the shear rate γ, so that again $k/(\rho d^3\gamma^2)$ disappears as a parameter, leaving

$$\frac{\tau d}{k} = f(\nu, \mu, \varepsilon). \tag{4.5}$$

Somewhere between these limits lies the elastic–inertial regime for which either the inertial scaling for the stress, $\tau/(\rho d^2\gamma^2)$, or the elastic scaling, $\tau d/k$, is appropriate

and for which $k/(\rho d^3\gamma^2)$ remains as a parameter. This will be used to precisely define the elastic–inertial regime. That is, elastic–inertial behaviour covers the region where both the elastic and inertial scalings $\tau d/k$, $\tau/(\rho d^2\gamma^2)$ are dependent on the parameter $k/(\rho d^3\gamma^2)$.

It is valuable then to consider both scalings for the stress as the deviation from the expected behaviour under each scaling can be used to detect the boundaries of the various flow regimes. To that end, figure 7 shows a logarithmic plot of the elastic scaling of the normal stress $\tau_{yy}d/k$ as a function of concentration, for three different values of the friction coefficient. In this scaling, the stress for a quasi-static (elastically dominated) flow will appear as a horizontal line. If the flow is inertially dominated, one would expect the stresses to be proportional to $\rho d^2\gamma^2$, which means that, when scaled as in figure 7, the slopes of the lines should be -1, which is indeed achieved at the larger values of $k/(\rho d^3\gamma^2)$. (A large $k/(\rho d^3\gamma^2)$ implies a small shear rate γ, which leads to the ironic conclusion that small shear rate flows are more 'rapid' than large shear rate flows.) Figure 8 shows the same data plotted logarithmically with the inertial scaling, $\tau_{yy}/(\rho d^2\gamma^2)$. Here if the lines are horizontal, the flow is behaving inertially and any slope in the lines indicates an elastic influence. In particular, for a quasi-static flow, the stresses τ_{yy} are independent of γ so that $\tau_{yy}/(\rho d^2\gamma^2)$ increases linearly proportional to $k/(\rho d^3\gamma^2)$ (i.e. with unit slope on these logarithmic plots). In all cases, an elastic–inertial behaviour is apparent for small $k/(\rho d^3\gamma^2)$, but for large $k/(\rho d^3\gamma^2)$ the flow again exhibits either an elastic or an inertial behaviour with a very sharp transition between the two. Note that it is difficult to discern the elastic–inertial regime in any of these plots simply because the baseline elastic behaviour so dominates the overall stress that the additional inertial stresses (which produce at most a factor of 3 variation in the stresses shown in figures 3–5) all but disappear when plotted logarithmically.

Now, examine the limit at large $k/(\rho d^3\gamma^2)$. Following the criteria in the last paragraph, notice that for $\mu = 0.5$ and 1.0, the material exhibits quasi-static behaviour for $\nu = 0.59$ and larger, while for $\mu = 0.1$, quasi-static behaviour is only observed for $\nu = 0.62$. Below $\nu = 0.58$, for $\mu = 0.5$ and 1.0 and below $\nu = 0.61$ for $\mu = 0.1$, the material appears to behave in a purely inertial fashion. The transition from elastic to inertial behaviour at these $k/(\rho d^3\gamma^2)$ is very rapid, occurring over at most a 2% change in concentration. In fact, the only cases in which a transitional behaviour is observed – that is cases where the data follow a trend lying somewhere between the elastic–quasi-static and pure inertial behaviours at large $k/(\rho d^3\gamma^2)$ – is at $\nu = 0.58$ for $\mu = 1.0$ and at $\nu = 0.61$ for $\mu = 0.1$. The $\mu = 0.5$ data show no mixed behaviour and a rapid transition between pure elastic and pure inertial behaviours occurs within a 1% change in the particle concentration. The two transitional cases can be recognized by comparing their behaviour in the two different scalings. Notice that when plotted with the elastic scaling in figure 7(*c*), the $\nu = 0.58$, $\mu = 1.0$ data appear to have a significant inertial component, yet, when plotted with the inertial scaling in figure 8(*c*), they seem to group with the elastic data. Collectively these illustrate their mixed nature.

This indicates that much of the difference between figures 6(*a*) and 6(*b*) is due to different physical origins of the stress; figure 6(*a*) is an elastically dominated stress, while figure 6(*b*) is inertially dominated. Despite this, note that long duration contacts are apparent in figure 6(*b*), indicating that the material is trying to form structures that are at least the precursors to force chains. However, the corresponding elastic stresses are much weaker than the inertially generated stresses and do not significantly affect the overall rheology.

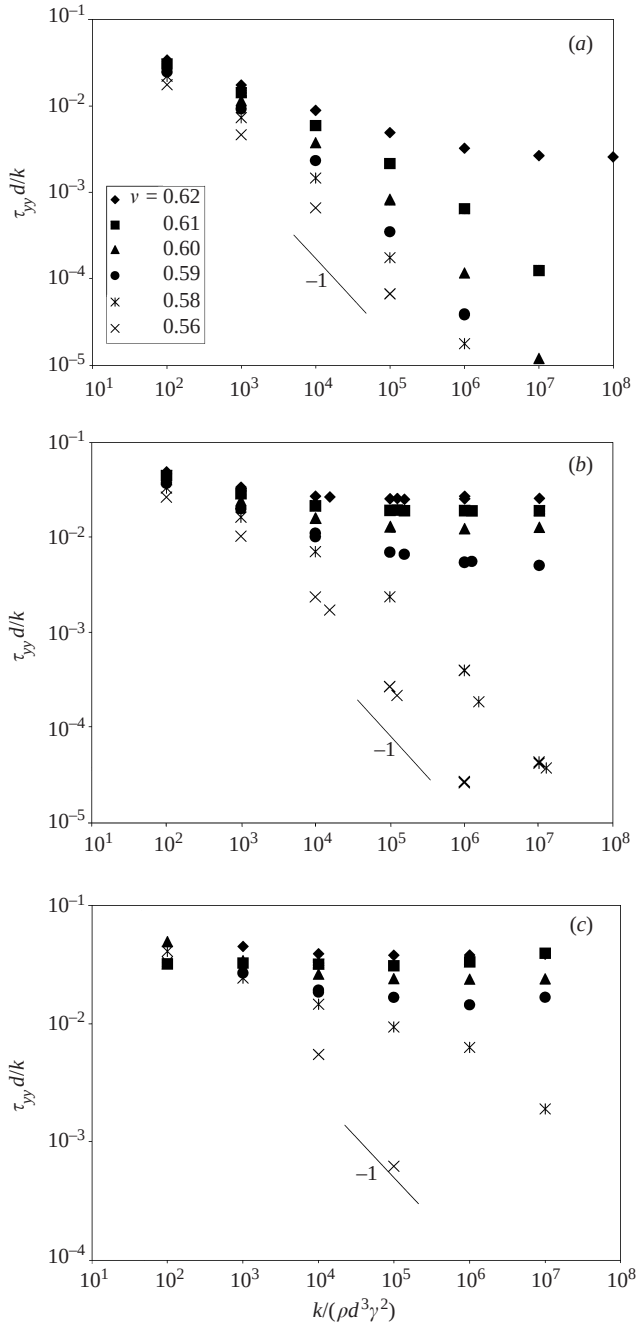

FIGURE 7. The effect of friction on the dimensionless normal stress $\tau_{yy}d/k$ for $\varepsilon = 0.7$. (*a*) $\mu = 0.1$, (*b*) $\mu = 0.5$, (*c*) $\mu = 1.0$. On these logarithmic scales, horizontal lines represent pure elastic behaviour and lines with slope -1 indicate inertial behaviour.

The narrow band of concentrations over which the transition between elastic and inertial flows occurs at large $k/(\rho d^3\gamma^2)$ suggests a percolation threshold at which the force chains form. Elastic–quasi-static behaviour is realized when these structures dominate the force transmission; the fluctuating forces are generated as

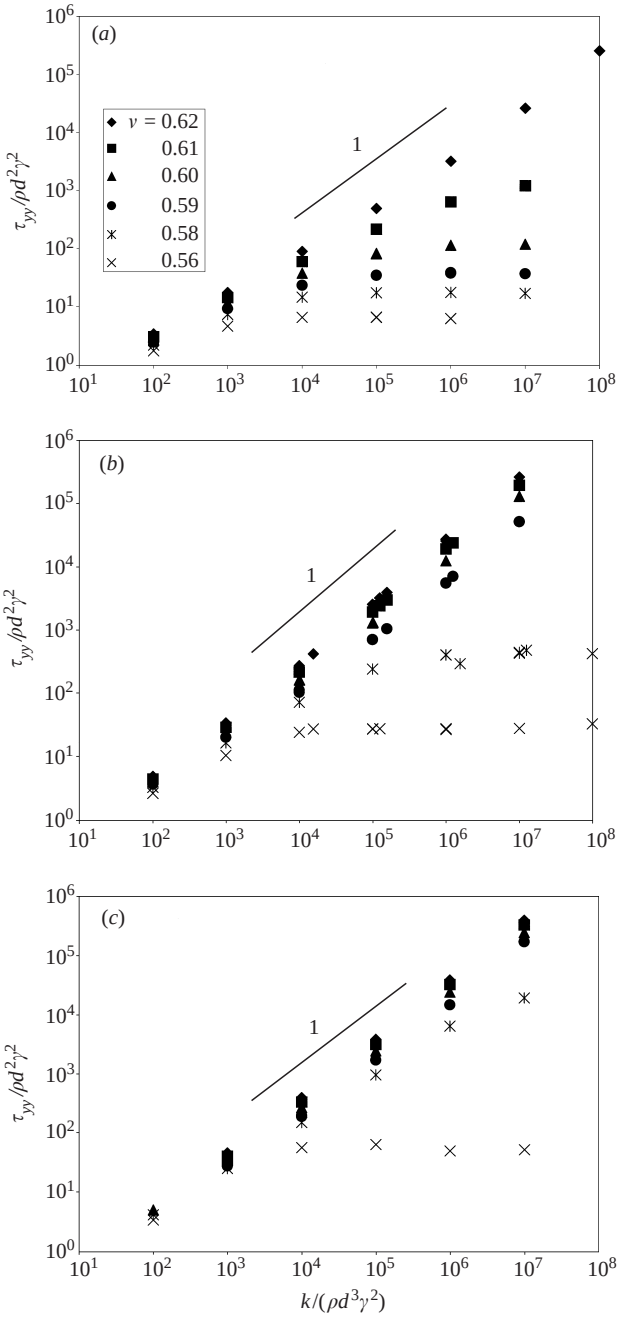

FIGURE 8. The same data as in figure 7 presented logarithmically in the inertial scaling. Here, horizontal lines indicate pure inertial behaviour while lines with slope 1 indicate that the stresses are nearly strain-rate independent. (*a*) $\mu = 0.1$, (*b*) $\mu = 0.5$, (*c*) $\mu = 1.0$.

these chains form, and are compressed and destroyed by the velocity gradient. At lower concentrations, the chains, if they form, quickly break so that particle inertia remains an important component of the momentum transport. If this is indeed a percolation behaviour, one might worry that these transition concentrations could be

strongly dependent on the system size. Thus, tests were performed at $k/(\rho d^3\gamma^2) = 10^7$ (at which the regime transition is accompanied by several orders of magnitude of stress change) on larger control volume sizes both by doubling the size in all three dimensions to $20 \times 20 \times 20$, and by extending one dimension by a factor of 10 to $10 \times 100 \times 10$. Such tests were performed on both sides of each observed transition. However, the measured stresses changed by less than 4% in all cases and changing the system size never caused a transition between elastic and inertial behaviour. Thus the transition concentrations appear to be insensitive to system size.

One should also note that as $k/(\rho d^3\gamma^2)$ is reduced, it is possible to observe a transition from pure inertial to elastic–inertial behaviour. This is most clearly seen in figure 8 as a transition from a sloping line at small $k/(\rho d^3\gamma^2)$ to a horizontal line at larger $k/(\rho d^3\gamma^2)$. This indicates that large shear rates can force the formation of force chains – a process that will be partially explained in the next section.

Also note that at a fixed concentration, ν, and fixed particle properties μ, d and k, there is no path between pure inertial and quasi-static behaviour by simply varying the shear rate, γ. For those conditions, changing γ is equivalent to changing $k/(\rho d^3\gamma^2)$ which can only cause a change from inertial–elastic and elastic–quasi-static behaviour or from elastic–inertial to inertial behaviour. This counters the generally accepted notion that, all else being equal, quasi-static behaviour can be observed at small shear rates and pure inertial behaviour observed at large shear rates. Instead, it appears that the transition from inertial to quasi-static behaviour can only be observed by changing the concentration, and then only at low shear rates (large $k/(\rho d^3\gamma^2)$).

As discussed in § 2, the ratio of the contact time to the binary collision time, t_c/T_{bc}, can be used as a probe to determine if the particle interactions are collisional. Any binary collision must have a contact time t_c, equal to the binary collision time, T_{bc}. However, if one envisions that particle contacts are caused by the shear flow forcing particles together in force chains, rotating the chains and finally breaking them, then one would expect the contact time t_c to be inversely proportional to the shear rate and independent of the binary collision time. Thus, when plotted in a log-log plot against $k/(\rho d^3\gamma^2)$, one expects t_c/T_{bc} to have a slope of $\frac{1}{2}$ in the elastic regimes. Figure 9 shows plots of t_c/T_{bc} for the three values of the friction coefficient. It can be clearly seen that at larger concentrations and at smaller values of $k/(\rho d^3\gamma^2)$, the data fall along a line with slope $\frac{1}{2}$ indicative of elastic behaviour. For smaller concentrations and larger values of $k/(\rho d^3\gamma^2)$, the values of t_c/T_{bc} become only weakly dependent on γ and approach $t_c/T_{bc} = 1$. This change in t_c/T_{bc} behaviour is another indicator of the transition from elastic to inertial behaviour. Notice that the change coincides with the transitions apparent in figures 7 and 8. In particular, note that one can observe a transition from elastic–inertial to pure inertial behaviour by increasing $k/(\rho d^3\gamma^2)$. Note also that even in the inertial range, t_c/T_{bc} can be much larger than 1, indicating that, even though the material is behaving inertially, it is not collisional and thus not strictly a rapid flow.

Rapid flow analyses assume that all particle interactions are binary so that the transport rate is governed by the time between collisions and thus by the granular temperature. If more than two particles are in simultaneous contact, transport can occur between the particles through elastic waves travelling across the contact points – a rate which is governed by the elastic properties and not by the granular temperature – and thus cannot be considered 'rapid'. Again, and somewhat ironically, t_c/T_{bc} goes to unity as $k/(\rho d^3\gamma^2)$ becomes large, indicating that the slower they shear, the more the flows become 'rapid'. This is one one reason why rapid flows are seldom observed under Earth's gravity. On one hand to meet the collisional criterion, they must shear

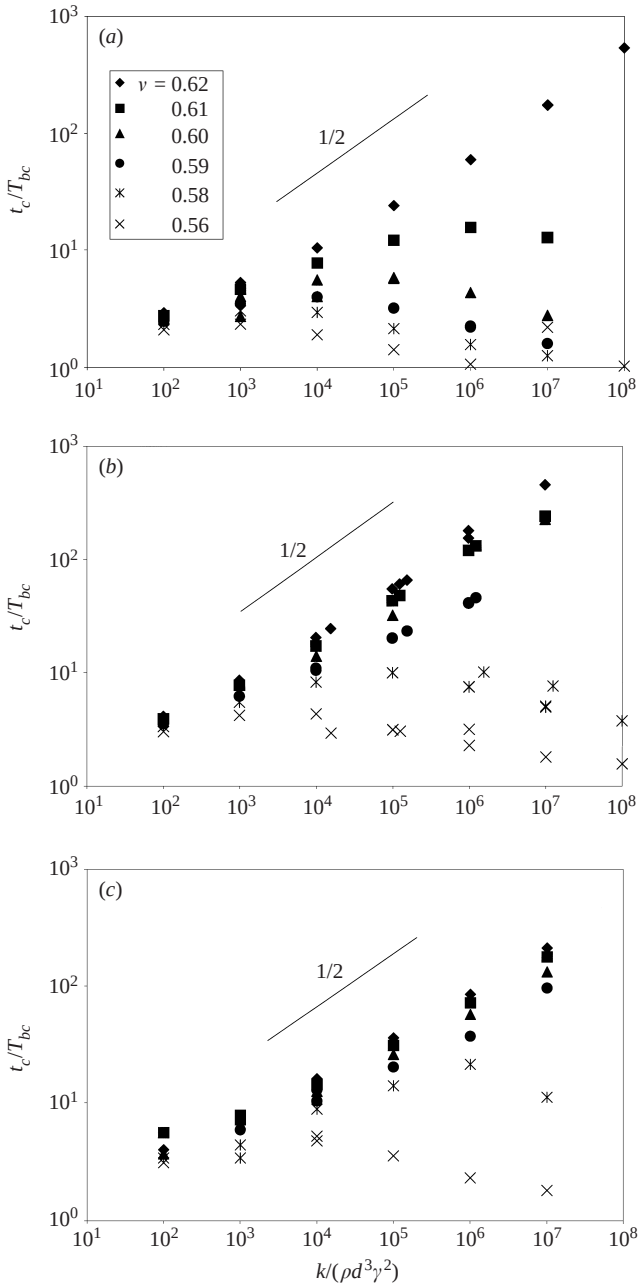

FIGURE 9. The ratio of the contact time to the binary collision time t_c/T_{bc} for $\varepsilon = 0.7$, as functions of $k/(\rho d^3\gamma^2)$. (*a*) $\mu = 0.1$, (*b*) $\mu = 0.5$, (*c*) $\mu = 1.0$. Collisional flows correspond to $t_c/T_{bc} = 1$. Flows dominated by force chains for which the contact time is controlled by the shear rate, should plot onto lines of slope 1/2.

slowly, but on the other, to generated large enough dispersive stresses to support the material against gravity, they must shear rapidly.

Note that this also illustrates the dual nature of the parameter $k/(\rho d^3\gamma^2)$ that was alluded to in the last section. In the elastic regime, quasi-static behaviour is observed

at large $k/(\rho d^3\gamma^2)$, indicating that this may be thought of as the zero shear rate ($k \to 0$) limit, while at slightly lower concentrations, in the inertial regime, flows become collisional at large $k/(\rho d^3\gamma^2)$ implying that this represents the rigid particle ($k \to \infty$) limit.

Collectively, this information allows us to create flowmaps of the various flow regimes. These are shown in figure 10 as functions of $k/(\rho d^3\gamma^2)$ for $\varepsilon = 0.7$ and the three values of the surface friction coefficient. In this plot, the transition from elastic–inertial to elastic–quasi-static behaviour was determined from plots such as figure 3 for each concentration, by drawing lines through the points corresponding to the two regimes and noting the value of $k/(\rho d^3\gamma^2)$ at which they intersect. The transition from elastic–inertial to inertial–non-collisional behaviour was determined by the points where the transition occurs in figures 7–8. In figure 7, this would be the point where the slope of the line for a given concentration became -1, indicative of inertial behaviour. In figure 8, this would be the point where the line for a given concentration shifted from sloping to horizontal. The transition from elastic–quasi-static to inertial–non-collisional behaviour was simply the concentration at which quasi-static behaviour was last observed for a given μ. Note that these figures reach lower values of the solid fraction than are seen in figures 7–9 as elastic–inertial behaviour was observed for concentrations as small as $\nu = 0.45$ for $\mu = 1.0$ and $k/(\rho d^3\gamma^2) = 100$.

More difficult to determine is when a flow can be regarded as 'collisional'. Strictly, a collisional flow corresponds to $t_c/T_{bc} = 1$ and any value larger than unity indicates non-collisional behaviour. In practice, there will always be simultaneous multiparticle interactions even if they occur with vanishing probability so that such an ideal case is never achievable. The question then arises of to what degree a small number of multiparticle interactions affect the flow's behaviour. Such a determination is well beyond the scope of this paper. Three lines have been added to figure 10 roughly pointing out the places where t_c/T_{bc} falls below 1.5, 1.25 and 1.1, so as to leave the determination up to the reader. Note that these lines generally rise with $k/(\rho d^3\gamma^2)$ indicating that the particle interactions are becoming more collisional at large $k/(\rho d^3\gamma^2)$. But notice that the lines flatten at the top indicating that at larger concentrations t_c/T_{bc} remains well above unity and gave no indication that it would ever fall no matter what the value of $k/(\rho d^3\gamma^2)$.

The prescribed values chosen here are very close to unity and were made based on small simulations run to try and understand how confinement by surrounding particles extends the collision time. In these simulations, it was imagined that two particles were undergoing collision, and at the moment of maximum compression, when the particles had ceased to approach one another, they were placed in intimate contact with a line of stationary particles. The confining particles were placed so that the distances between their centres were exactly a particle diameter, so that their surfaces were in contact but no forces were generated; only the original colliding particles overlapped and experienced a force. In such a case, the collision will be lengthened due to the necessity of pushing away the surrounding particles. However, the collisions were not found to be lengthened to any large degree. For example, with a single confining particle on each side, the collision is lengthened to $t_c/T_{bc} = 1.03$. In fact, with an infinite number of confining particles, the collision is lengthened to $t_c/T_{bc} = 1.08$. In the latter case, the collisional energy becomes an elastic wave travelling down the line of particles, and because the wave never reflects before the end of the original collision, the original collision is unaware of the length of the line of confining particles. (Actually, this limit is reached with as few as three confining

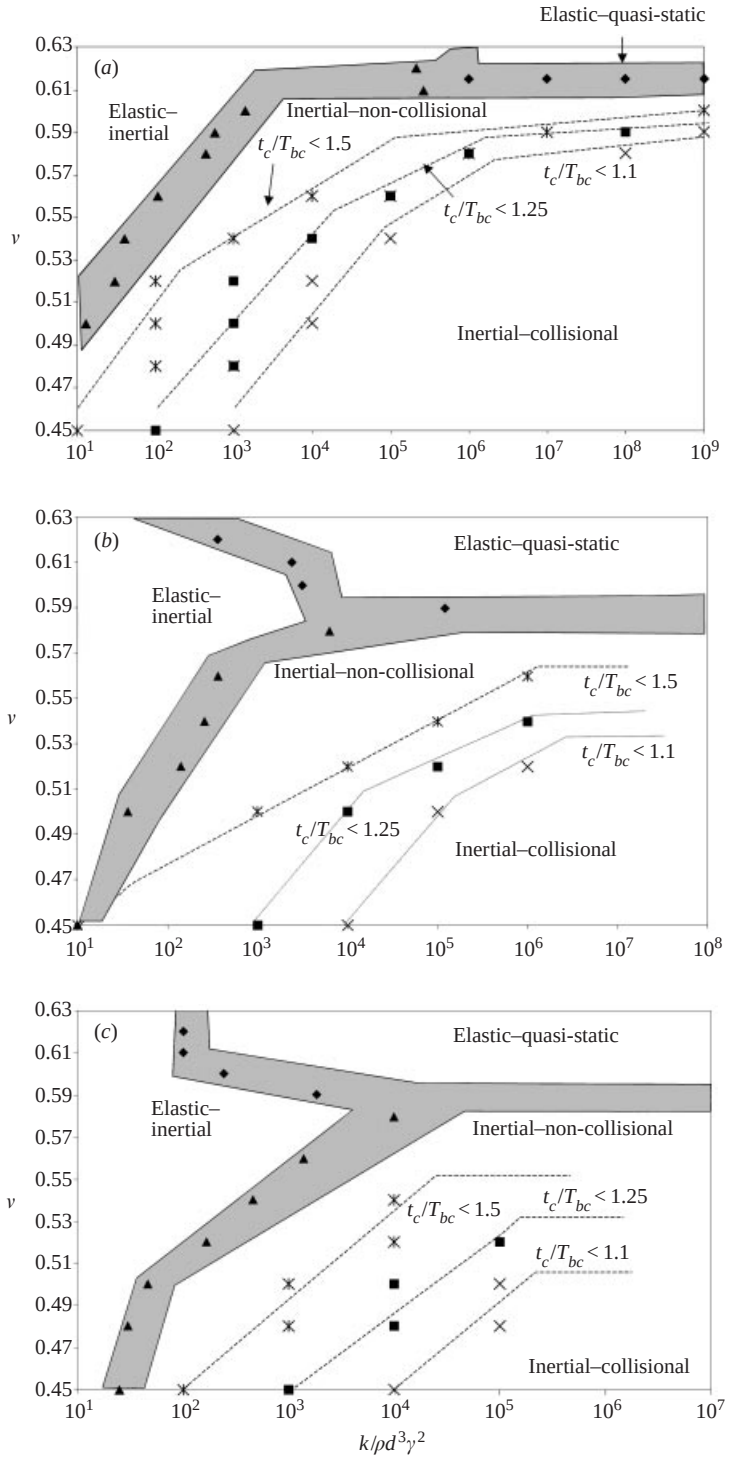

FIGURE 10. Flowmaps of the various flow regimes for $\varepsilon = 0.7$: (*a*) $\mu = 0.1$, (*b*) $\mu = 0.5$, (*c*) $\mu = 1.0$.

particles on each side.) In such a case, there is a transport of momentum over infinite distances that is both non-collisional and independent of the granular temperature. On that basis, it seems quite reasonable to assume that $t_c/T_{bc} = 1.1$ is an upper limit to collisional behaviour. But again, this is a subject worthy of further study. In contrast it should be noted that in the elastic regimes, the contact times are of the order $t_c/T_{bc} = 100$–1000.

5. Interpretations of the parameter $k/(\rho d^3\gamma^2)$

Bathurst & Rothenburg (1988) showed that for randomly packed spheres with linear contacts, the Young's modulus varies as

$$E \propto \frac{nk}{d}, \tag{5.1}$$

where n is the coordination number (the average number of contacts between particles) which in practice can vary from 0 to about 6. (Bathurst and Rothenburg's expression for three-dimensional assemblies appears only at the end of the paper and contains an undetermined definite integral, but the above scaling is still apparent in their equation.) This means that

$$n\left(\frac{k}{\rho d}\right) \propto \frac{E}{\rho} \propto (\text{sound speed})^2. \tag{5.2}$$

But since γd is a shear velocity, the grouping

$$\frac{k}{\rho d^3\gamma^2} = \left(\frac{k}{\rho d}\right)\left(\frac{1}{\gamma d}\right)^2 \propto \left(\frac{\text{sound speed}}{\text{shear velocity}}\right)^2 \propto \left(\frac{1}{\text{Mach number}}\right)^2 \tag{5.3}$$

can be interpreted as an inverse square Mach number based on the shear velocity γd. Examining figure 2, one sees that the stress ratio can be observed to drop with $k/(\rho d^3\gamma^2)$, until a value of $k/(\rho d^3\gamma^2) = 10^4$, which implies a Mach number of the order of 10^{-2}.

The sound speed gives us a means to calculate appropriate values for the stiffness k. In loose sand, the sound speed is of the order of $100\,\mathrm{m\,s^{-1}}$ (Richart, Woods & Hall 1970). To within an order of magnitude then

$$\frac{k}{\rho d} \approx 10^4\,\mathrm{m^2\,s^{-2}}. \tag{5.4}$$

This means that to be in the elastic–inertial regime, $(d^2\gamma^2) \sim 1\,\mathrm{m^2\,s^{-2}}$. Thus if one assumes particles of 1 mm size, the shear rate would have to be close to $\gamma \sim 1000\,\mathrm{s^{-1}}$, which would never be encountered in practice as the impacts would probably shatter the particles. Even if one includes the effect of coordination number, n, in the calculation, this would at best drop this estimate by a factor of 3 at most. Of course larger particles would give a correspondingly smaller limiting shear rate. Following this logic, the rapid granular shear flow experiments of Wang & Campbell (1992) using 3 mm glass spheres at shear rates of $\sim 100\,\mathrm{s^{-1}}$ would roughly correspond to $k/(\rho d^3\gamma^2) = 10^4$. Even the largest values studied here, $k/(\rho d^3\gamma^2) = 10^7$, correspond to $3\,\mathrm{s^{-1}}$ of shear for the same particles. (Because of that realization, test cases were run at values up to $k/(\rho d^3\gamma^2) = 10^{10}$, particularly around the transitions to and from elastic behaviour, but no noticeable changes in behaviour were observed.) However, smaller values of k and larger diameters quickly reduce the value of $k/(\rho d^3\gamma^2)$. For example commercial plastics have moduli that are generally two orders of magnitude

smaller than quartz and are often formed into large $\sim$ 5 mm pellets, and thus should exhibit elastic–inertial behaviour at an easily reachable 5 s^{-1} of shear. And of course there are many materials such as cigarettes, encapsulated pharmaceuticals and foodstuffs, that are softer still, and make the inertial–elastic regime even more accessible.

The conclusion that can be drawn here is that realistic values of $k/(\rho d^3\gamma^2)$ can be quite large so that the elastic–inertial regime is difficult to reach for many common materials. This has interesting implications for the discussion in the last section. If one looks at the data in figures 7 and 8 at the large $k/(\rho d^3\gamma^2)$ which are likely to be encountered, it appears that either pure inertial or pure quasi-static behaviour is observed depending on the concentration, with little or no transition region between them. Furthermore, most flows that are to be encountered under Earth's gravity are most likely to be out in the quasi-static range of figure 2.

This discussion begs a complementary interpretation of the parameter $k/(\rho d^3\gamma^2)$. In standard fluid mechanics, a large Mach number is indicative of a compressible material and, not surprisingly, the same interpretation can be made for $k/(\rho d^3\gamma^2)$. Basically, a small $k/(\rho d^3\gamma^2)$ (analogous to a large Mach number) means that there is enough inertial energy in the particles to cause significant deformation of the particles against the stiffness k. If all the inertial energy were to be converted into the potential energy of a contact, it would cause an overlap δ_I so that

$$m(\Delta v)^2 \sim \rho d^3 (d\gamma)^2 \sim \tfrac{1}{2} k \delta_I^2. \tag{5.5}$$

Rearranging:

$$\left(\frac{\delta_I}{d}\right)^2 \sim \frac{\rho d^3\gamma^2}{k}. \tag{5.6}$$

Thus, $k/(\rho d^3\gamma^2)$ can be thought of as the inverse square of the particle overlap that is generated by the flow inertia, distinguished from that generated by quasi-static mechanisms such as the compression of force chains. In that sense, flows at small $k/(\rho d^3\gamma^2)$, like flows at significant Mach number, are fluid dynamically compressible.

The appearance of this compressibility explains the anecdotal observation made during the course of these simulations that at small $k/(\rho d^3\gamma^2)$ it was possible to obtain a uniform shear flow at larger concentrations than was possible at large $k/(\rho d^3\gamma^2)$. For example, at $k/(\rho d^3\gamma^2) = 100$, the material exhibited uniform shear at $\nu = 0.63$, while at $k/(\rho d^3\gamma^2) = 100\,000$, it exhibiting a shear-banding behaviour. At such significant 'compressibilities' the particles just compress, deform and push past their neighbours. As there is nothing in rapid granular flow theory that accounts for compressibility effects it also helps explain the observation in figure 7 that the incompressible large-$k/(\rho d^3\gamma^2)$ flows are more 'rapid' than their larger shear rate, but compressible small-$k/(\rho d^3\gamma^2)$ counterparts.

Finally, there is one more interpretation of $k/(\rho d^3\gamma^2)$ that yields insight into why the flow can be observed to transition from inertial to elastic–inertial behaviour as $k/(\rho d^3\gamma^2)$ is reduced. First, consider the expression for the coefficient of restitution ε in (2.1), which can be inverted to obtain

$$\frac{D^2}{2mk} = \left(\frac{D^2}{m^2}\right)\left(\frac{m}{2k}\right) = \frac{1}{(\pi/\ln\varepsilon)^2 + 1}. \tag{5.7}$$

This can be recognized as the ratio of the two terms in the denominator of equation (2.2) for the binary contact time T_{bc}. From (5.7) it can be seen that in most cases

$(D^2/m^2) \ll (2k/m)$. For example, for $\varepsilon = 0.7$, used here, $(D^2/m^2) = 0.013(2k/m)$. In such cases, the binary contact time is dominated by the stiffness k so that

$$T_{bc} \approx \frac{\pi}{\sqrt{2k/m}} = \pi\sqrt{\frac{\rho d^3}{12k}} \propto \sqrt{\frac{\rho d^3}{k}}. \tag{5.8}$$

Hence:

$$\frac{k}{\rho d^3 \gamma^2} \propto \frac{1}{(T_{bc}\gamma)^2}. \tag{5.9}$$

In other words, $k/(\rho d^3\gamma^2)$ may be thought of as the square of the ratio of the time between shear-rate-induced particle impacts, which goes like the inverse shear rate $\sim 1/\gamma$ (note this same interpretation applies in rapid flow theory as the collision rate varies as the square root of the granular temperature which in turn varies as $1/\gamma$), to the time it takes the contact forces to drive the particles apart, T_{bc}. Thus, at small values of $k/(\rho d^3\gamma^2)$, particles are being forced together at a rate that is becoming comparable to the collision time. This allows force chains to form at smaller values of ν than one would anticipate. In turn, this explains why a material can exhibit elastic–inertial behaviour at small $k/(\rho d^3\gamma^2)$ and inertial behaviour at large $k/(\rho d^3\gamma^2)$. It also explains why the scaled duration of the peaks in figure 6(c) is slightly longer than that in figure 6(a). The peak duration will consist of the rate at which the shear motion creates rotates and destroys the force chains. All those process but the final chain destruction are governed by the shear rate γ. The time it takes the particle elasticity to break apart a collapsing chain is proportional to the binary contact time T_{bc}. At small values of $k/(\rho d^3\gamma^2)$, T_{bc} becomes a significant fraction of the chain's lifetime, resulting in slightly larger dimensionless durations, when as in figure 6, the duration is scaled with the shear rate.

6. The effect of non-linear contact stiffness in the elastic–quasi-static regime

By now it should be obvious that the contact model has a strong effect on the rheological behaviour in the elastic region. This problem is compounded by the fact that real contacts generally behave nonlinearly so that the force generated is not linearly proportional to the contact displacement. Thus, this section will try to assess the effects of such nonlinearity on the scaling behaviour in the elastic–quasi-static regime.

So far we have only considered linear contact springs, for which the force generated on a contact is

$$F = k\delta, \tag{6.1}$$

where δ is the overlap between the particles. Now if one were to assume that the contact between particles behaved in a Hertzian fashion, then when placed in this context, the force would vary as

$$F = k_H\delta^{3/2}, \tag{6.2}$$

where the constant k_H is a function of the elastic properties of the particle and local radii of curvature of the contacts. Many people anticipate that materials should behave in a Hertzian fashion simply because Hertz theory is a solution to linear elastic theory. However, that does not appear to be borne out by measurements. The sound speed in a granular material depends on the elastic properties of the bulk material (not the individual particles) and can be used as a probe of the contact

dynamics. As pointed out by Goddard (1990), the experimental evidence (e.g. Richart 1978; Richart *et al.* 1970) indicates that the power of δ is actually larger than $3/2$. Goddard (1990) suggested that this was due to the fact that the particles actually interacted across sharp asperities and, using known elastic solutions, proposed a model that eventually transitions to Hertzian behaviour as the stresses became large enough to press out the asperities. This type of behaviour appears to be generally borne out by the direct load cell measurements of Mullier, Tuzun & Walton 1991; however, these showed a more complicated behaviour, starting with a power smaller than $3/2$, followed by a region where the power was larger than $3/2$ and finally settling into a power equal to $3/2$. One can also make a case that linear models are also adequate as it should always be possible to linearize the stiffness around a base overlap δ_0 which is a function of the local stress levels, and indeed such ideas are commonly used in sound propagation models. Also Thornton (1997) has shown that an elastic–plastic particle will exhibit a stiffness that is approximately linear although the unloading stiffness will be different and larger than the loading stiffness. (This is similar to the two-spring model first used in simulations by Walton & Braun 1986.)

There is no simple answer to these questions especially since the behaviour of contacts undoubtedly varies from material to material, but it should be possible to achieve some general understanding of the behaviour of nonlinear contacts by investigating a generic contact with behaviour

$$F = k_0 \delta^n \tag{6.3}$$

and an associated stiffness

$$k = k_0 \delta^{n-1}. \tag{6.4}$$

This stiffness is zero until there is some overlap, δ, and increases from then on (notice that k_0, k_H and k will all have different dimensions).

What effect will this have on the rheology of the material? The first thing to notice is that since the stiffness is initially zero and that the expected overlaps are generally small, the nonlinear models initially produce a less stiff material than their linear counterparts. If one imagines a shear flow with particles that are continually in contact, the flow will press particles together resulting in some sort of average displacement $\langle \delta \rangle$ that generates the stress response. If one assumes that the force is distributed over the area of a particle, then

$$\tau = \frac{k_0 \langle \delta \rangle^n}{d^2}. \tag{6.5}$$

Solving for $\langle \delta \rangle / d$ gives

$$\frac{\langle \delta \rangle}{d} = \left(\frac{\tau d^{2-n}}{k_0^2} \right)^{1/n}. \tag{6.6}$$

Note that one expects that the degree of deformation $\langle \delta \rangle / d$ induced by the shear would be a function largely of the concentration. Note also that all the n, i.e. all of the signs of nonlinearity, appear on the right-hand side. Thus, one might expect that

$$\left(\frac{\tau d^{2-n}}{k_0^2} \right)^{1/n} \tag{6.7}$$

is a scaling for the stress that takes the nonlinearity into account. This should then be

an appropriate dimensionless stress, at least in the elastic–quasi-static regime when all forces are generated by such overlaps.

The predicted effects of n are then quite interesting. For $n = 2$, the parameter, and hence the stresses, are independent of particle diameter. For $n > 2$ the stress τ will, at constant values of this parameter, increase with particle diameter and for $n < 2$, the stress will decrease with particle diameter. For a linear contact ($n = 1$) the above reduces to the elastic scaling, $\tau d/k$.

The nonlinearity will also affect the parameter, $k/(\rho d^3\gamma^2)$, where now $k = k_0\delta^{n-1}$. In fact one can go through an analysis similar to that used to find equation (5.6) to obtain

$$\frac{\delta_I}{d} = \left(\frac{k_0}{\rho d^{4-n}\gamma^2}\right)^{\frac{1}{1-n}}, \tag{6.8}$$

where δ_I represents the overlap generated by the inertia of the particle. One might expect that the right-hand side represents the equivalent of $k/(\rho d^3\gamma^2)$ for nonlinear contacts (and reduces to that in the linear case, $n = 1$) but tests show that this is not the case – at least not for the large concentrations studied here. The characteristic overlap δ, which determines the characteristic stiffness $k = k_0\delta^{n-1}$, is a function of whatever generates the stresses and is the result of quasi-static deformation and inertial effects. While these two contributions can be separated in a linear system, the same cannot be done for nonlinear contacts. Consequently, it is not possible to find a characteristic value of k to use when defining an appropriate equivalent to $k/(\rho d^3\gamma^2)$. (The only way to do this would be to estimate the value of δ from the local stress state to yield an appropriate k, but the resulting equivalent to $k/(\rho d^3\gamma^2)$ would then be a dimensionless stress and graphs such as figures 2–9 would be plots of dimensionless stress against dimensionless stress.) However, the conclusions drawn in the last section are still valid: that the likely values of $k/(\rho d^3\gamma^2)$ are large, and at large concentrations, quasi-static behaviour (independent of $k/(\rho d^3\gamma^2)$) can be anticipated. Consequently, it is possible to perform tests of the nonlinear effects simply at large values of $k/(\rho d^3\gamma^2)$, without requiring precise control over the exact value of $k/(\rho d^3\gamma^2)$. (Such a region was determined by first running at small values of γ, and then estimating k for the stress state, to check that the effective $k/(\rho d^3\gamma^2)$ was larger than 10^6.) The analysis around equation (6.7) assumes that the material is reacting elastically to the shear deformation. One would then expect this scaling to hold when the system is behaving elastically and break down at smaller concentrations when the flow transitions to inertial behaviour. A plot of the scaled yy stress component is shown in figure 11. At each concentration, the particle size was varied by a factor of 4 and the stiffness constant k_0 was varied by a factor of 10. This scaling collapses the data at the largest concentrations, but very quickly fails at concentrations below about $\nu = 0.59$, where the data scatter with both the nonlinearity factor n and with particle size, d. This is to be expected as the linear stiffness data anticipate inertial behaviour below $\nu = 0.59$. Nonetheless (6.7) does represent a scaling for nonlinear contacts throughout the elastic–quasi-static regime.

7. Conclusions

This paper investigates the high density limit of granular flow in which the elastic properties of the particles become important in determining the overall rheology. The elastic properties make their appearance through the contact stiffness k, which is the

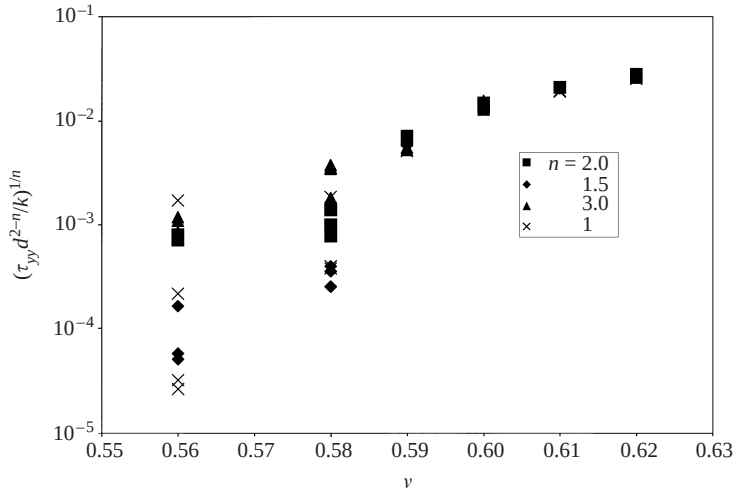

FIGURE 11. A check on the scaling for the nonlinear contact models. For this figure the particle surface friction was held fixed at $\mu = 0.5$. Note that the scaling holds for large concentrations of $\nu > 0.59$ which previously delineated the elastic region for a linear stiffness.

property that most directly governs the elastic properties of the bulk material. Note that k is not solely a function of the elastic properties of the solid material that makes up the particles, but also depends strongly on the geometry of the interparticle contacts. Hence one cannot directly relate the elastic properties of the bulk granular material to the properties of the solid material of which the individual granules are composed.

At large concentrations, the stresses are generated by elastic deformations of the bulk material and as such should be related to the bulk elastic properties. A convenient dimensionless stress is then $\tau d/k$, which scales the stress with the interparticle stiffness k that governs the bulk elastic properties. (This parameter can be interpreted as the ratio of the length of the contact deformation to the particle diameter.) Dimensional analysis also provides an appropriate dimensionless parameter $k/(\rho d^3\gamma^2)$, that scales the shear rate γ with the interparticle stiffness, k. (This parameter may be interpreted as the ratio of the that portion of the contact deformation that is inertially induced to the particle diameter.) There are two regimes in this limit. In the 'elastic–inertial' regime, the stresses scale elastically, but also increase with shear rate; this is encountered at small $k/(\rho d^3\gamma^2)$. In the 'elastic–quasi-static' regime, the stresses again scale elastically but are strain-rate independent; this corresponds to large $k/(\rho d^3\gamma^2)$. Magnitude estimates of $k/(\rho d^3\gamma^2)$ for common materials indicate that the elastic–inertial regime is only reachable for very soft materials or very large particles and is not accessible to many standard granular solids such as 1 mm sand.

It has long been known that the load applied to a granular material is not evenly distributed among the constituent particles. Instead it is carried mostly along 'force chains', highly loaded networks of particles that span the system, while many particles experience little or none of the applied force. These force chains determine the elastic response of the bulk material. The fact that the stresses scale with the elastic properties of the bulk material as $\tau d/k$ indicates that they are generated by particle deformation within the force chains. As the material shears, these force

chains are formed and rotate and eventually break under the applied loads and the effects of shear, a process observed by Howell, Behringer & Veje (1999*a*, *b*). This is supported by observations that the stresses fluctuate and that the normal stresses are strongly affected by the particle surface friction, μ. Large surface friction leads to stronger force chains and consequently larger stresses can be generated before the chain breaks.

Note that the effect of the surface friction μ may only be important for the spherical particles studied here. Non-spherical particles will tend to lock together and form strong internal structures by virtue of their shape alone. In fact one would expect this to be more important than the surface friction in determining the force chain strength for non-spherical particles.

As the concentrations are reduced the material can rapidly transition from 'elastic–quasi-static' strain-rate-independent behaviour to a fully inertial behaviour where the stresses are independent of the elastic properties. At large $k/(\rho d^3\gamma^2)$, where the strain rates and the corresponding inertial stresses are small, such a transition can cause a dramatic change in the stresses. In that regime, a 2% drop in concentration is observed to cause nearly a three orders of magnitude change in the stresses. This suggests a percolation threshold for the force chains that support the material when it behaves quasi-statically. Furthermore the threshold appears to be strongly dependent on friction. At $\mu = 0.1$, elastic–quasi-static behaviour is observed only above $\nu = 0.61$ but for $\mu = 1.0$ the threshold has dropped to $\nu = 0.58$. These huge stress changes, accompanying such small changes in concentration, indicate that granular materials near these limiting concentrations are prone to instabilities; natural fluctuations in the concentration can cause the flow to locally transition between flow regimes with huge changes in the stress. Such instabilities have been reported in the shear cell studies of Savage & Sayed (1984), Hanes & Inman (1985) and Wang & Campbell (1992) and cause severe vibration of the test cell.

It was also noted that a transition from pure inertial to elastic–inertial behaviour can be observed for small values of $k/(\rho d^3\gamma^2)$, at surprisingly small concentrations. In these studies such a transition was observed at concentrations as small as $\nu = 0.45$. As small $k/(\rho d^3\gamma^2)$ implies large shear rates, this indicates that the large shear rate can force the formation of force chains. This can be understood through an analysis of the parameter $k/(\rho d^3\gamma^2)$, that indicates that it is proportional to the square of the ratio of the inverse shear rate to the binary contact time. In other words, it may be thought of as the ratio of the time between collisions ($\sim 1/\gamma$), which forces particles together, to the binary collision time T_{bc}, which controls the rate at which the interparticle elastic forces can separate the particles. Thus, for small values of $k/(\rho d^3\gamma^2)$, particles are driven together at rates close to the rate at which they are elastically pushed apart, allowing force chains to form at remarkably small concentrations.

Previously it was generally understood that quasi-static behaviour would be observed at small shear rates and inertial behaviour at large shear rates. These results show this not to be the case. *At fixed concentration, there is no path between quasi-static and rapid behaviour*. Changing the shear rate with all other properties fixed caused transitions between elastic–quasi-static and elastic–inertial or between inertial and elastic–inertial. Only varying the concentration, could force a transition between elastic–quasi-static and inertial behaviours.

This work was largely motivated by previous studies of landslides, hopper flows and the 'phase-change' between solid and fluid behaviour. These collectively indicated that the stress ratio τ_{xy}/τ_{yy} increased with the shear rate γ, a behaviour

that is unexpected for standard quasi-static and rapid flow models. These simulations demonstrated that when in the elastic–inertial regime, the stress ratio τ_{xy}/τ_{yy} decreases with $k/(\rho d^3\gamma^2)$ and thus does indeed increase with the shear rate.

These results should serve as a warning to users of soft-particle simulations. Because it speeds the execution of the simulation, there is a tendency to use unrealistically soft particles. Generally it has been argued that as long as the particle overlaps are small, this should not affect the flow. However, these studies put another restriction on the particle stiffness, as reducing k reduces $k/(\rho d^3\gamma^2)$ which can cause an unrealistic change from elastic–quasi-static to elastic–inertial behaviour.

Finally, nonlinear contact models for which the interparticle force varies as $k_0\delta^n$ were investigated. Inertial effects are not easy to scale in this case, but in the elastic–quasi-static regime, the nonlinear effects could be taken into account by scaling the stresses as $(\tau d^{2-n}/k_0)^{1/n}$.

The latter stage of this work was supported by the National Aeronautics and Space Administration under grant number NAG3-2358. Special thanks to Sasha Potapov for his help with the simulation development and to Gustavo Joseph for his help with the figures.

REFERENCES

Babic, M., Shen, H. H. & Shen, H. T. 1990 The stress tensor in granular shear flows of uniform, deformable disks at high solids concentrations. *J. Fluid Mech.* **219**, 81–118.

Bagnold, R. A. 1954 Experiments on a gravity-free dispersion of large solid particles in a Newtonian fluid under shear. *Proc. R. Soc. Lond.* A **225**, 49–63.

Bathurst, R. J. & Rothenburg, L. 1988 Micromechanical aspects of isotropic granular assemblies with linear contact interactions. *Trans. ASME: J. Appl. Mech.* **55**, 17–23.

Bonnecaze, R. T. & Brady, J. F. 1992 Yield stresses in electrorheological fluids. *J. Rheology* **36**, 73–115.

Campbell, C. S. 1986 Computer simulation of rapid granular flows. *Proc. 10th Natl Congr. of App. Mech., Austin Texas, June 1986*, pp. 327–338. ASME.

Campbell, C. S. 1989 The stress tensor for simple shear flows of a granular material. *J. Fluid Mech.* **203**, 449–473.

Campbell, C. S. 1990 Rapid granular flows. *Annu. Rev. Fluid Mech.* **22**, 57–92.

Campbell, C. S. 1993 The transition from fluid-like to solid-like behaviour in granular flows. In *Powders and Grains 93* (ed. C. Thornton), pp. 289–294. A. A. Balkema.

Campbell, C. S. 1997*a* Self-diffusion in granular shear flows. *J. Fluid Mech.* **348**, 85–101.

Campbell, C. S. 1997*b* Computer simulation of powder flows. In *Powder Technology Handbook*, 2nd Edn (ed. K. Gotoh, H. Masuda & K. Higashitani), pp. 777–794. Marcell Dekker.

Campbell, C. S. 2001*a* Granular flows in the elastic limit. In *The Granular State* (ed. S. Sen & M. L. Hunt), pp. BB4.4.1–BB4.4.12. Materials Research Society, Warrendale, PA, 2001.

Campbell, C. S. 2001*b* Granular flows in the elastic limit. In *IAS Special Publication 31: Sediment Transport and Deposition by Particulate Gravity Currents; Proc. Conf. on Particular Gravity Currents, Leeds, UK, September, 1998*. Blackwell-Science (to appear).

Campbell, C. S., Cleary, P. & Hopkins, M. A. 1995 Large landslide simulations: global deformation, velocities and basal friction. *J. Geophys. Res.* **100**, 8267–8283.

Campbell, C. S. & Gong, A. 1986 The stress tensor in a two-dimensional granular shear flow. *J. Fluid Mech.* **164**, 107–125.

Campbell, C. S. & Zhang, Y. 1992 Interfaces between fluid-like and solid-like behaviour in granular flows. In *Advances in Micromechanics of Granular Materials – Proc. Second US/Japan Seminar on the Micromechanics of Granular Materials, Potsdam, New York, August 5–9, 1991* (ed. H. H. Shen, M. Satake, M. Mehrabadi, C. S. Chang & C. S. Campbell), pp. 261–270. Elsevier.

Cauchy, A. L. 1828 De la pression ou tension dans un systeme de points materiels. *Exercise de Mathematique*, vol. 3, p. 213.

Cundall, P. A. & Strack, O. D. L. 1979 A discrete numerical model for granular assemblies. *Geotechnique* **29**, 47–65.

Drescher, A. & De Josselin de Jong, G. 1972 Photoelastic verification of a mechanical model for the flow of a granular material. *J. Mech. Phys. Solids* **20**, 337–351.

Glasser, B. J. & Goldhirsch, I. 2001 Scale dependence, correlations, and fluctuations of stresses in rapid granular flows. *Phys. Fluids* **13**, 407–420.

Goddard, J. D. 1990 Nonlinear elasticity and pressure-dependent wave speeds in granular media. *Proc. R. Soc. Lond.* A **430**, 105–131.

Goldhirsch, I. & Tan, M. L. 1996 The single-particle distribution function for rapid granular shear flows of smooth inelastic disks. *Phys. Fluids* **8**, 1752–1763.

Goldshtein, A. & Shapiro, M. 1995 Mechanics of collisional motion of granular-materials. Part 1. General hydrodynamic equations. *J. Fluid Mech.* **282**, 75–114.

Hanes, D. M. & Inman, D. L. 1985 Observations of rapidly flowing granular fluid flow. *J. Fluid Mech.* **150**, 357–380.

Herrmann, H. J. & Luding, S. 1998 Modeling granular media on the computer. *Cont. Mech. Therm.* **10**, 189–231.

Howell, D. W., Behringer, R. P. & Veje, C. T. 1999*a* Fluctuations in granular media. *Chaos* **9**, 559–572.

Howell, D. W., Behringer, R. P. & Veje, C. T. 1999*b* Stress fluctuations in a 2D granular Couette experiment: A continuous transition. *Phys. Rev. Lett.* **26**, 5241–5244.

Hunt, M. L., Zenit, R., Campbell, C. S. & Brennen, C. E. 2002 Revisting the 1954 suspension experiments of R. A. Bagnold. *J. Fluid Mech.* **452**, 1–24.

Hwang, H. & Hutter, K. 1995 A new kinetic model for rapid granular flow. *Cont. Mech. Therm.* **7**, 357–384.

Jackson, R. 1983 Some mathematical and physical aspects of continuum models for the motion of granular materials. In *Theory of Dispersed Multiphase Flow* (ed. R. E. Meyer), pp. 291–337. Academic.

Jenkins, J. T. & Askari, E. 1991 Boundary conditions for granular flows: phase interfaces. *J. Fluid Mech.* **223**, 497–508.

Jenkins, J. T. & Richman, M. W. 1985 Grad's 13-moment system for a dense gas of inelastic spheres. *Arch. Rat. Mech. Anal.* **87**, 355–377.

Lees, A. W. & Edwards, S. F. 1972 The computer study of transport processes under extreme conditions. *J. Phys. C: Solid State Phys.* **5**, 1921–1929.

Lun, C. K. K., Savage, S. B., Jeffrey, D. J. & Chepurniy, N. 1984 Kinetic theories for granular flow: inelastic particles in Couette flow and slightly inelastic particles in a general flow field. *J. Fluid Mech.* **140**, 223–256.

Miller, B., O'Hern, C. & Behringer, R. P. 1996 Stress fluctuations for continuously sheared granular materials. *Phys. Rev. Lett.* **77**, 3110–3113.

Mueth, D. M., Jaeger, H. M. & Nagel, S. R. 1998 Force distribution in a granular medium. *Phys. Rev.* E **57**, 3164–3169.

Mullier, M., Tuzun, U. & Walton, O. R. 1991 A single-particle friction cell for measuring contact frictional-properties of granular materials. *Powder Technol.* **65**, 61–74.

Potapov, A. V. & Campbell, C. S. 1996 Computer simulation of hopper flows. *Phys. Fluids* **8**, 2884–2894.

Richart, F. E. Jr 1978 Field and laboratory measurements of dynamic soil properties. In *Dynamic Response and Wave propagation in Soils* (ed. B. Prange). A. A. Balkema.

Richart, F. E., Woods, R. D. & Hall, J. P. 1970 *Vibration of Soils and Foundations.* Prentice Hall.

Savage, S. B. & Dai, R. 1993 Studies of granular shear flows, wall slip velocities, layering and self-diffusion. *Mech. Mater.* **16**, 225–238.

Savage, S. B. & Sayed, M. 1984 Stresses developed by dry cohesionless granular materials in an annular shear cell. *J. Fluid Mech.* **142**, 391–430.

Thornton, C. 1997 Coefficient of restitution for collinear collisions of elastic perfectly plastic spheres. *Trans. ASME: J. Appl. Mech.* **64**, 383–386.

Walton, O. R. 1993 Numerical simulation of inelastic, frictional particle-particle interactions. In *Particulate Two-Phase Flow* (ed. M. C. Roco). Butterworth-Heinemann.

WALTON, O. R. & BRAUN, R. L. 1986 Viscosity and temperature calculations for shearing assemblies of inelastic, frictional disks. *J. Rheol.* **30**, 949–980.

WANG, D. G. & CAMPBELL, C. S. 1992 Reynolds analogy for a shearing granular material. *J. Fluid Mech.* **244**, 527–546.

ZHANG, Y. & CAMPBELL, C. S. 1992 The interface between fluid-like and solid-like behaviour in two-dimensional granular flows. *J. Fluid Mech.* **237**, 541–568.